Available online at www.sciencedirect.com

SCIENCE DIRECT®

Tectonophysics 388 (2004) 33–45

TECTONOPHYSICS

www.elsevier.com/locate/tecto

Lower crustal fluid distribution in the northeastern Japan arc revealed by high-resolution 3D seismic tomography

Makoto Matsubara[a,*], Naoshi Hirata[b], Hiroshi Sato[b], Shin'ichi Sakai[b]

[a]National Research Institute for Earth Science and Disaster Prevention 3-1, Tennodai, Tsukuba, Ibaraki 305-0006, Japan
[b]The Earthquake Research Institute, the University of Tokyo 1-1-1 Yayoi, Bunkyo-ku, Tokyo 113-0032, Japan

Received 10 September 2003; received in revised form 21 January 2004; accepted 13 June 2004
Available online 26 August 2004

Abstract

The Ou Backbone Range strikes northwards through the central northeastern Japan arc and is bounded on both sides by the active reverse Uwandaira and Sen'ya faults. We have applied a traveltime inversion method (seismic tomography) with spatial velocity correlation to active and passive seismic data in order to investigate a three-dimensional (3-D) velocity structure. The data set contains 33,993 P- and 18,483 S-wave arrivals from 706 natural sources and 40 blasts, as well as 2803 P-wave traveltime data from 10 explosions detonated during the 1997 controlled source experiment. The traveltime inversion reveals a zone beneath the Ou Backbone Range in which P-wave velocities (V_P) are approximately 6–8% lower than the average velocity at equivalent depths. The low V_P and a low V_P to S-wave velocity (V_S) ratio (V_P/V_S) of about 1.65 suggest the presence of aqueous fluids in the middle crust.

Keywords: Island arc; Volcanic front; Middle crustal aqueous fluids; Tomographic method; Northeastern Japan arc

1. Introduction

The northeastern Japan arc is one of the typical and most active convergent plate boundaries with an active volcanic chain parallel to the arc and the Japan Trench (Fig. 1, Sato, 1994). The structures of the arc crust are important to understand active tectonics ongoing in the subduction zone. The generation mechanism of a large intra-arc earthquake is one of the most important issues to be addressed in the intra-arc tectonics.

Ague et al. (1998) found that liquid migrating into less permeable crust might trigger the intraplate earthquakes. It is important to distinguish aqueous liquid from molten rock in the crust to understand mechanical properties of the crust. We observe lateral variation of volcanic activity along the volcanic chain and the large intra-arc earthquakes correlate with thermal distribution: large earthquakes occurred where few volcanoes exist.

Seismic methods, including reflection and refraction seismic methods (Iwasaki et al., 1999, 2001; Sato

* Corresponding author. Tel.: +81 29 863 7674; fax: +81 29 860 2317.
E-mail address: mkmatsu@bosai.go.jp (M. Matsubara).

0040-1951/$ - see front matter © 2004 Elsevier B.V. All rights reserved.
doi:10.1016/j.tecto.2004.07.046

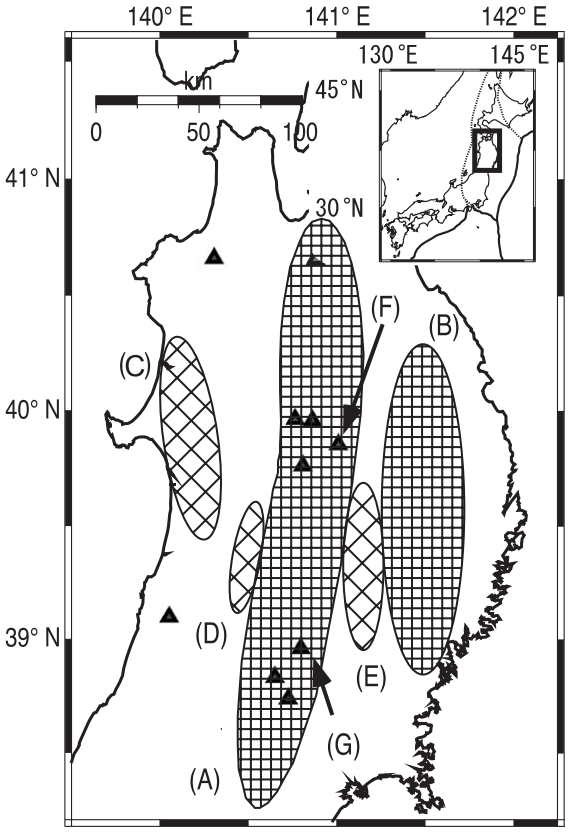

Fig. 1. Location map showing the modern tectonic features of the northeastern Japan arc. (A) Ou Backbone Range, (B) Kitakami Mountains, (C) Akita–Noshiro Plain, (D) Yokote basin, (E) Kitakami Low Land, (F) Mt. Iwate, and (G) Mt. Kurikoma.

et al., 2002) and a magnetotelluric method (Ogawa et al., 2001), basically revealed two-dimensional structure in detail. To study the relationship between the structure and seismicity, however, we should clarify a three-dimensional (3-D) structure. In the present study, we present the three-dimensional fluid distribution in the middle crust in the northeastern Japan arc along the volcanic front by a tomographic method with a densely distributed seismic array data.

2. Geological setting

The crust of the northeastern Japan arc was produced by accretionary processes in the Paleozoic to Mesozoic era and by a large amount of intrusion of granitic rocks in the late Cretaceous. The northeastern Japan arc was rifted away from Eurasian continent at 25–15 Ma, accompanied by the formation of grabens and half-grabens and volcanic eruptions in the back arc. Since the Pliocene, crustal shortening formed folds and narrow uplifts bounded by reverse faults in the back arc of the northeastern Japan arc (Sato, 1994).

Along the Ou Backbone Range, felsic Valles-type calderas were formed by voluminous magmatic intrusions in late Miocene to Pliocene (Sato and Amano, 1991; Yoshida, 2001). The formation of these calderas ended by 1.8 Ma (Sato and Amano, 1991). Since late Pliocene, the Backbone Range was elevated by reverse faulting up to 1000 m above the sea level.

The Ou Backbone Range strikes northwards through the northeastern Japan arc (Figs. 1 and 2). Although a volcanic front runs along the Backbone Range, the large earthquakes and active faults are concentrated in the areas where few active volcanoes exist. The central part of the Backbone Range between Mt. Iwate and Mt. Kurikoma is bounded by two active reverse faults, the Uwandaira and Sen'ya faults. The active reverse Kawafune fault runs across the Backbone Range in NE–SW direction. The Riku-u earthquake of 1896 (Mj 7.2) produced surface breaks along the preexisting Sen'ya and Kawafune faults (Yamasaki, 1896).

Iwasaki et al. (2001) revealed the two-dimensional velocity structure across the arc by a refraction method. They noted that the crust beneath the Backbone Range is thick and relatively low in velocity as compared to the forearc crust. S-wave reflectors (Hori et al., 1999) and prominent seismic scatterers (Asano et al., 1999) are also reported at the depths of 5–15 km beneath the Backbone Range.

3. Seismic array experiments

Between October 1997 and June 1999, several Japanese university research groups conducted an intensive seismic observation campaign to investigate crustal structure and seismotectonics in the central northeastern Japan arc using both passive and active sources (Hasegawa and Hirata, 1999). The campaign included the Joint Seismic Observation (JSO; Research Group for the Seismicity and Structure of NE Honshu, Japan, 1998) and a dense seismic array observation (DSO) of microearthquakes using off-line

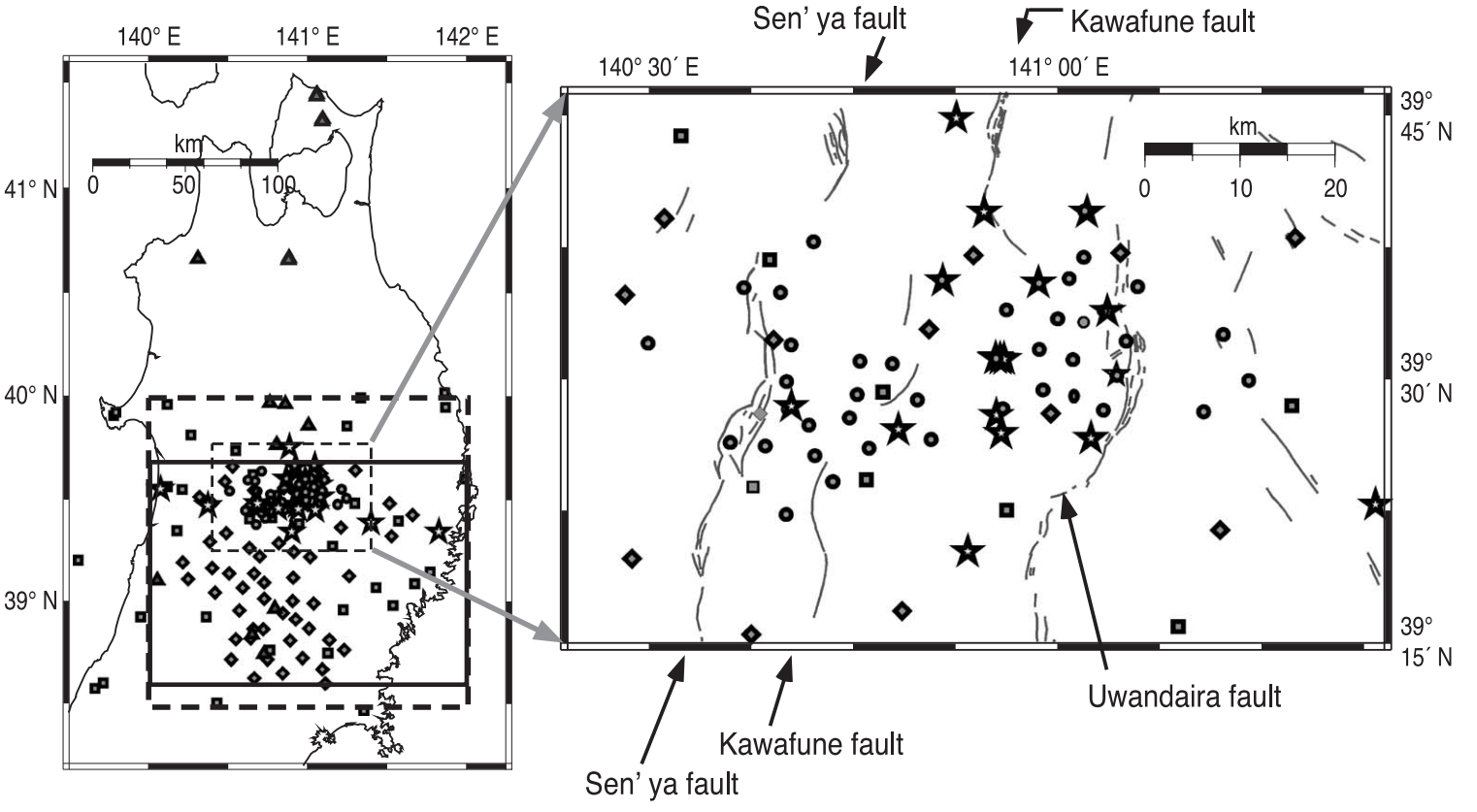

Fig. 2. Distribution of seismic station deployed in the Joint Seismic Observation (JSO) and the dense microseismic observation (DSO) with the Senya, Kawafune, and Uwandaira active reverse faults. Circles, diamonds, and squares denote off-line, temporary telemetry, and permanent telemetry stations, respectively. Stars show explosions by RGES in 1997 and 1998 (Iwasaki et al., 1999, 2001). Triangles denote active volcanoes. A box with thin broken lines denotes the area of the left map. A box with thick broken lines and a box with thick solid lines show the areas of Figs. 3 and 4, respectively.

seismic stations in and around the Ou Backbone Range.

As part of the JSO, besides 42 permanent telemetered stations we deployed 50 temporary telemetered seismic stations for the entire period of the program with an average station spacing of 10–20 km (Fig. 2). A three-component seismograph was installed in each station.

To obtain more detailed crustal velocity structures, we need more densely deployed seismic stations than the JSO. The DSO consists of 43 three-component portable seismographs operated between 14 July and 2 October 1998 in and around the central part of the Ou Backbone Range. The DSO array had an average station spacing of 2–3 km. The recorders included a Global Positioning System (GPS) receiver which provided a precise clock signal for the timing of recording every 6 h.

The Research Group for Explosion Seismology (RGES) performed an extensive onshore–offshore wide-angle seismic experiment across the northeastern Japan arc in 1997 and imaged the structure and deformation of the mid- and lower crust (Iwasaki et al., 2001). They also denoted 13 explosive charges within the DSO array on the eastern side of the Ou Backbone Range on 10 August 1998 (Iwasaki et al., 1999) that were recorded by the DSO instruments.

4. Data

The telemetered data from the JSO were routinely processed to locate earthquakes (Urabe, 1994). From October 1997 to June 1999, we determined 13,429 events within the region of interest (37–42°N, 137.5–142.5°E, 0–650 km depth), of which 448 events with a magnitude larger than 3.0 were carefully examined for the traveltime inversion. These events produced 23,450 P- and 13,827 S-wave arrivals (Fig. 3a).

The continuously recorded DSO data were edited into event-by-event data used to locate 298 earthquakes beneath the array (38.5–40.0°N, 139.9–142°E, 0–160 km depth; Fig. 3b). We picked 7341 P- and 4656 S-wave arrivals observed at 135 stations including both the off-line and telemetry stations from the 298 events, which included natural earthquakes, RGES shots, and quarry blasts.

We also used the 2803 P-wave traveltime data from 10 explosive shots in 1997 (Fig. 3a,b) with bathymetry corrections obtained by the RGES (1999) for traveltime inversion. They picked almost all P-wave traveltime data from 10 shots to 287 stations.

5. Traveltime inversion

We used a traveltime inversion method (Zhao et al., 1992) with spatial correlation of velocities (Matsubara et al., 2001) to determine the velocity structure. In the original grid-type tomographic method (Zhao et al., 1992), the resolution of the images is equal to the grid spacing. We should place more than two grid nodes in the resolvable smallest size of heterogeneity considering the Nyquist wavelength to avoid spatial aliasing. It is more realistic to use as many grid nodes as possible for a representing heterogeneous velocity distribution. However, the increasing of grid nodes introduces an instability in the tomographic image having an artificially rough structure. We have introduced correlation among velocities at surrounding grid nodes to regulate the solution (Matsubara et al., 2001). We can correlate velocity perturbations to expand the effective area. This is the meaning of the spatial correlation. We could have more realistic velocity distribution than the conventional grid-type tomographic method. We also correlate velocities to stay close to the initial model using likelihood in damped least square method.

We used an initial velocity model simplified from the two-dimensional (2-D) velocity model derived from refraction study (Iwasaki et al., 2001). Each layer is assigned a one-dimensional velocity distribution obtained by averaging Iwasaki's 2-D model in that depth interval.

We divide the medium into four layers by three seismic velocity discontinuities, which represent the

Fig. 3. Distribution of hypocenters during the JSO and DSO observation. Scale of the vertical direction is half of that of horizontal direction. Solid diamonds and triangles denote off-line stations and on-line telemetry stations. (a) Hypocenters determined by the telemetry stations from October 1997 to June 1999. (b) Hypocenters determined by the off-line and telemetry stations between 14 July and 2 October 1998. The area shown in (b) is indicated by a box in (a).

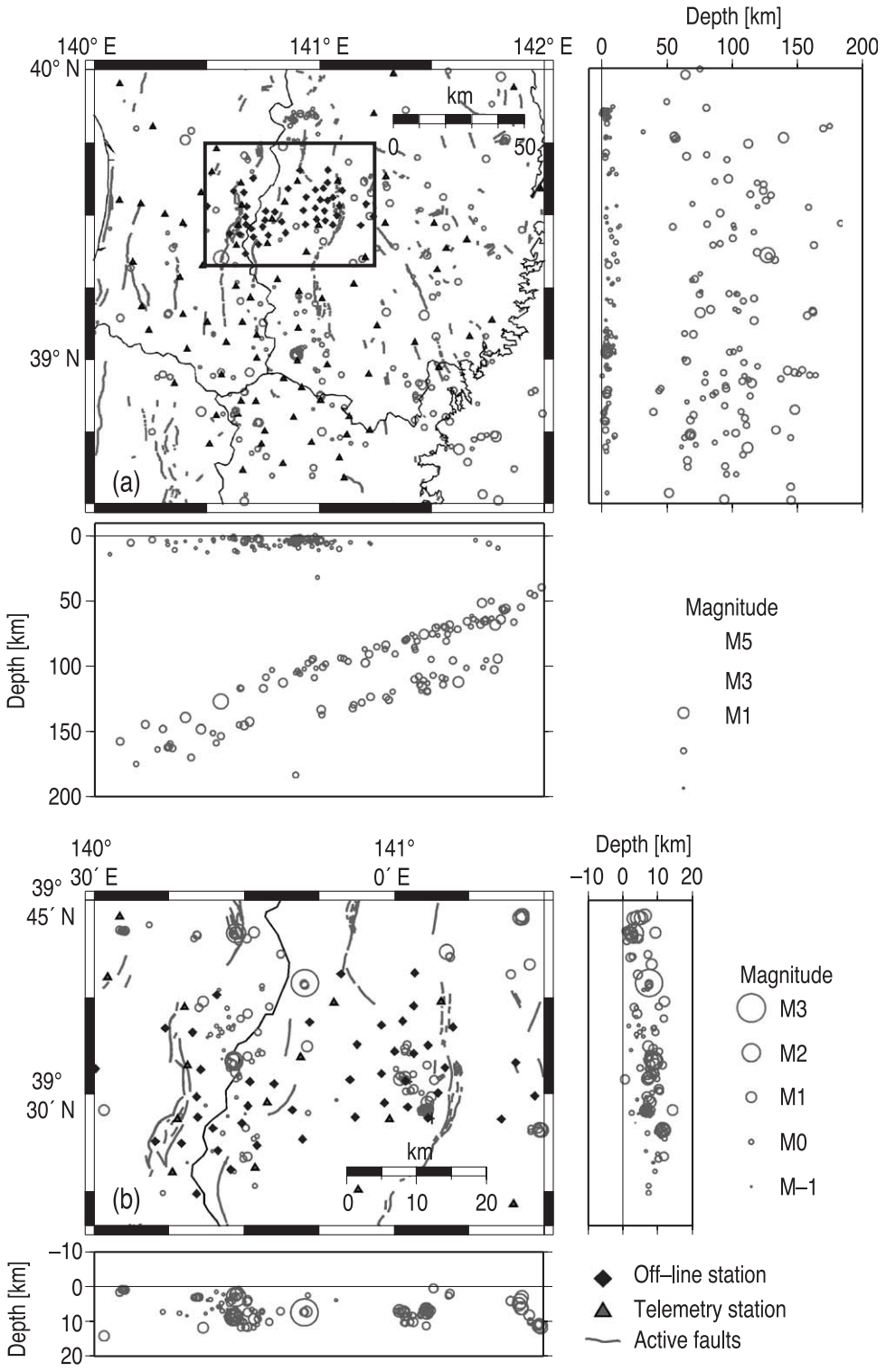
140° E
141° E
142° E
40° N
39° N
km
0
50
(a)
Depth [km]
0
50
100
150
200
Magnitude
M5
M3
M1
140°
30′ E
141°
0′ E
39°
45′ N
39°
30′ N
(b)
–10
0
10
20
M3
M2
M1
M0
M–1
Off–line station
Telemetry station
Active faults

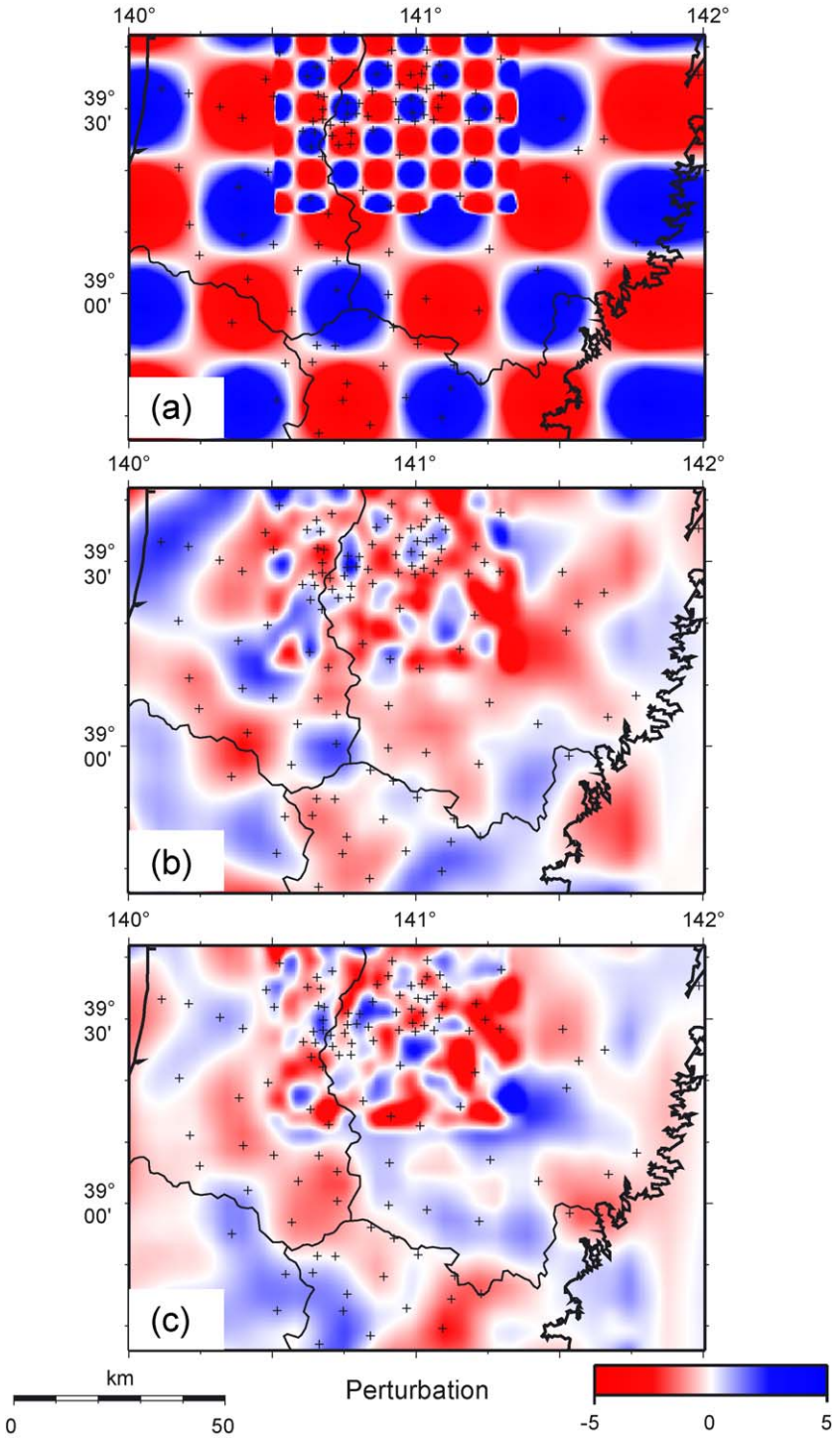

Fig. 4. Checkerboard pattern for the resolution test. (a) Assumed checkerboard pattern for P-wave velocity for checkerboard resolution test. The assumed pattern for S-wave is the opposite sign of that for P-wave. (b) Results of checkerboard resolution test for P-wave (c) Same as (b) except for those for S-wave. Pluses denote the seismic stations.

Conrad and Moho discontinuities (Iwasaki et al., 2001), and the upper boundary of the Pacific plate (Zhao and Hasegawa, 1993). We assume a three-dimensional (3-D) grid net for each layer to represent the velocity structure.

We subdivide the uppermost layer, which is presumed to correspond to the upper crust, into two zones in order to image the area beneath the DSO in detail. Within the area, a horizontal spacing of the grid nodes is 2.5 km, whereas outside the DSO it is 5.0 km. Grid nodes are located at depths of −1.0, 1.5, 4.0, 9.0, 14.0, 19.0, and 24.0 km. In the lower crust, a horizontal spacing of the grid nodes is 10 km and grid nodes are placed at depths of 15.0, 22.0, and 29.0 km. In the mantle wedge and the Pacific plate, the grid nodes have 30-km spacing.

The traveltime inversion algorithm solved for the latitude, longitude, depth and origin time of 706 earthquakes, and the latitude, longitude and origin time of 27 quarry blasts (a total of 706×4+27×3=2905 hypocentral parameters), as well as 18,539 P- and 17,916 S-wave slowness parameters.

6. Results

We assumed the ±5% checkerboard pattern changing with the grid sizes (Fig. 4a). (Fig. 4b,c) show the

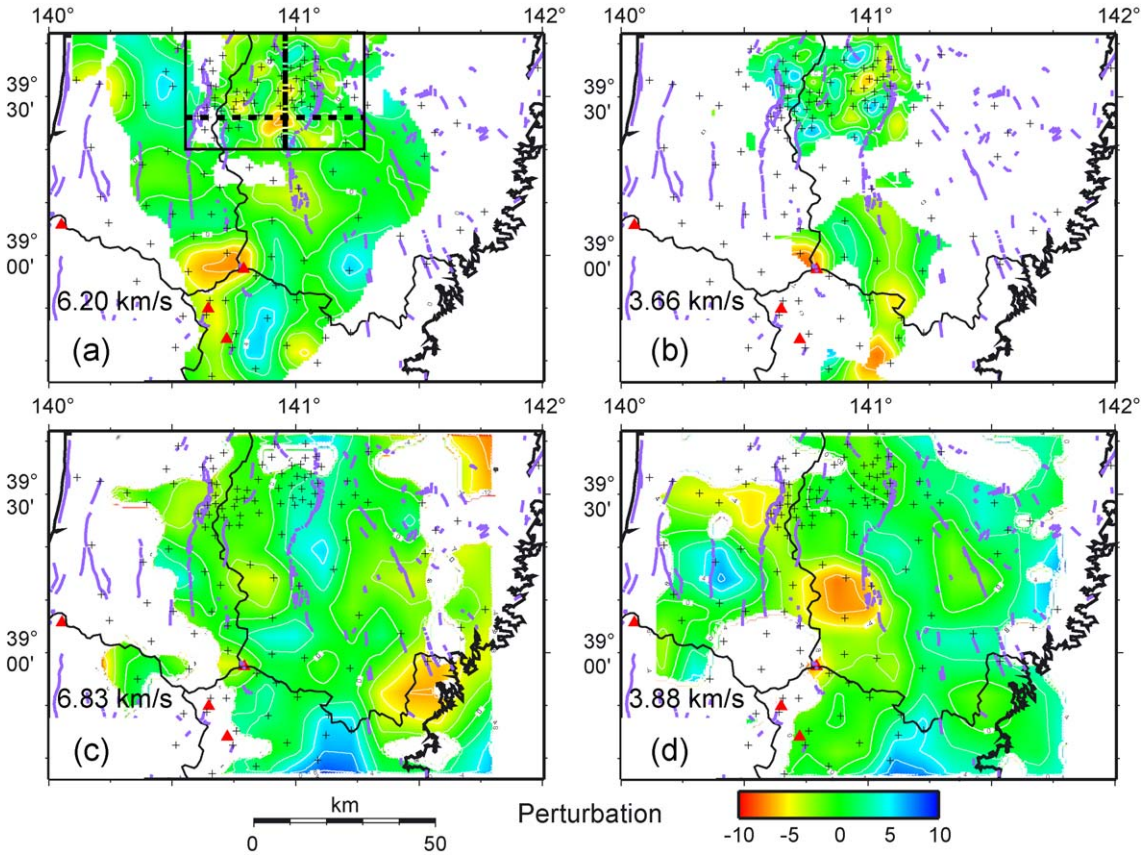

Fig. 5. Horizontal velocity perturbation model. Numerals at the bottom left-hand corner are the average V_P or V_S at those depths. Pluses denote the seismic stations. Purple lines denote the traces of active faults at the surface. Red triangles denote the active volcanoes. Contour interval is 2%. White masked areas are not resolved well. (a) Horizontal velocity perturbation model of V_P at a depth of 10 km in the upper crust. (b) Same as (a) except for that for V_S. (c) Horizontal velocity perturbation model of V_P at a depth of 25 km in the lower crust beneath the Tohoku area. (d) Same as (c) except for that for V_S. A thick horizontal broken line in (a) denotes cross sections of Fig. 6a–d and a vertical line in (e) denotes a cross section of Fig. 6e. A box in (e) shows the area of Fig. 7a.

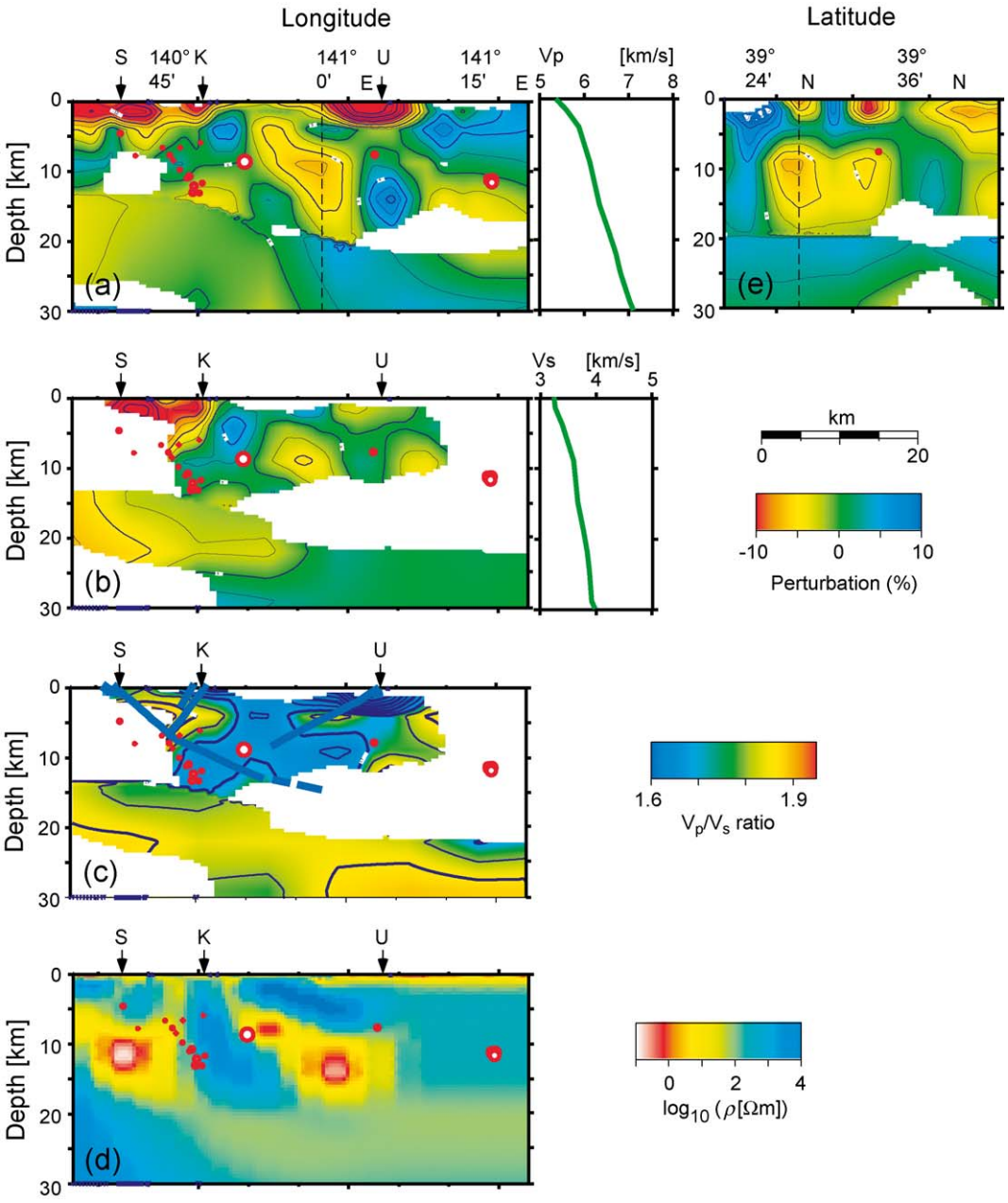

Fig. 6. Vertical cross section showing comparison among V_P, V_S, and resisitivity. (a) Vertical E–W cross section of V_P perturbation model at a latitude of 39.43°N. Box on the right-hand side shows the horizontally averaged V_P structure. Arrows denote the surface traces of the 'S'enya, 'K'awafune, and 'U'wandaira active reverse fauls. Contour interval is 2%. White masked areas are not resolved well. (b) Vertical E–W cross section of V_S perturbation model at a latitude of 39.43°N. Box on the right-hand side shows the horizontally averaged V_S structure. Arrows and white areas correspond to those in (a). Contour interval is 2%. (c) Vertical E–W cross section of V_P/V_S ratio model at a latitude of 39.43°N. Solid blue lines denote schematic diagram of the active faults (Hirata et al., 1999; Sato et al., 2002). Arrows correspond to those in (a). Contour interval is 0.05. (d) Vertical E–W cross section of resistivity model at a latitude of 39.43°N derived from the magnetotelluric methods (after Ogawa et al., 2001). Arrows correspond to those in (a). (e) Vertical N–S cross section of V_P at a longitude of 140.95°E. Contour interval is 2%. White masked areas are not resolved well.

results of the checkerboard resolution tests for P- and S-wave, respectively. We added random noise to the synthetic traveltime data with zero mean and standard deviations of 0.05 and 0.1 s for P- and S-wave, respectively, as estimated uncertainty of the picks derived from the emergent onset of waves. Lateral

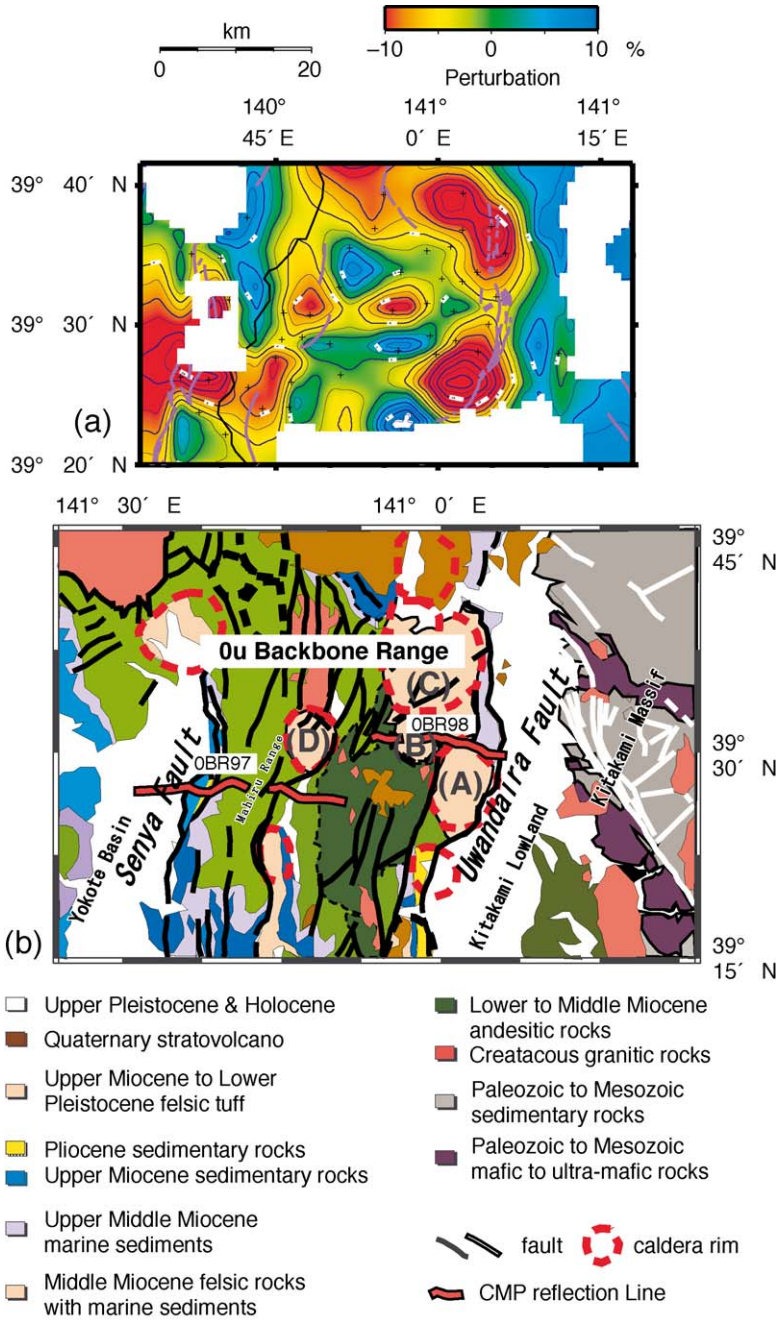

Fig. 7. Comparison between the velocity distribution and a surface geology. (a) V_P perturbation models at a depth of 1.5 km. White masked areas in (a) are not resolved well. (b) Generalized geological map of the central part of Ou Backbone Range (after Sato et al., 2002).

velocity variations in and around the Ou Backbone Range are well resolved at depths of 1.5–10.0 km. Horizontal resolution near the upper/lower crust interface is poor, but velocity perturbations in the lower crust beneath the Ou Backbone Range and the Kitakami Lowland are well resolved.

The traveltime inversion reduced the root mean square (RMS) of P-wave traveltime residual from 0.343 to 0.186 s (45%) in 19 iterations. The corresponding decrease in RMS residual for the S-wave data was from 0.441 to 0.280 s (36%).

Fig. 5a and b shows maps of the estimated velocity perturbation of a P-wave velocity (V_P) and an S-wave velocity (V_S) with respect to the average velocity at a depth of 10 km in the upper crust beneath the northeastern Japan arc. In the uppermost crust, the inversion results in negative (low) velocity perturbations of 4–8% beneath the Kitakami Lowland, Yokote Basin, Noshiro–Akita Plain, and Mt. Kurikoma. The interior of the Kitakami mountainous region is underlain by material with velocities 2–5% higher than the average 1-D model. In the lower crust, the inversion produces positive (high) velocity perturbations of 2–4% beneath the Kitakami Lowland and a low velocity zone beneath the Ou Backbone Range and further west (Fig. 5c,d).

Beneath the area surrounding the DSO, the inversion produces negative (low) P- and S-wave velocity perturbations of similar magnitude (5–10%) at shallow depth beneath the Kitakami Lowland (Figs. 6a,b and 7a). The corresponding perturbations beneath the Ou Backbone Range are also negative, with magnitudes of 4–8% (P-wave, Fig. 6a) and 2–6% (S-wave, Fig. 6b), and delineate a zone at depths of 5–15 km that extends for approximately 10 km in the E–W direction (Fig. 6a) and 18 km in the N–S direction (Fig. 6e).

7. Discussion

7.1. Velocity structure of the northeastern Japan arc

The V_P and V_S models given by the present inversion are, in general, similar to those shown by Nakajima et al. (2001). The low V_P zones in the upper crust are beneath the Ou Backbone Range and the west of it and those in the lower crust are beneath the Kitakami Mountains and the Ou Backbone Range. We obtained a more detailed structure beneath the Ou Backbone Range bounded by the Sen'ya and the Uwandaira active faults.

The low velocity zone in the upper most crust (6 km/s at 8–13 km depth) deepens to the west from the fore-arc to the back arc side. This is consistent with the result of the refraction survey (Iwasaki et al., 2001).

The origin of high/low velocity zone can be attributed to the difference of material composition, temperature, or existence of liquid, and so on. Although we can obtain information of substances at the surface from the geology, it is difficult to obtain that information at depth.

Fig. 5a shows horizontal P-wave velocity perturbations at a depth of 10 km. We compare the velocity distribution at that depth with a Curie depth map (Fig. 8; Okubo et al., 1989), which has information at depths of 7–15 km. The low velocity zone (5.9–6.1 km/s at 10 km depth, Fig. 5a) corresponds to shallow Curie depth (8 km). Then the temperature of the low velocity zone can be considered to be high. Thus, the low velocity zone suggests relatively high temperature at these depths.

7.2. Distribution of low velocity zones and calderas

Along the Ou Backbone Range, felsic Valles-type calderas were formed by voluminous magmatic intrusions in late Miocene to Pliocene. Fig. 7 shows comparison of distribution of calderas and that of P-

Fig. 8. Curie depth contour map of the northeastern Japan arc (after Okubo et al., 1989). Numerals are Curie depths in km. Hatched areas are those with a Curie depth deeper than 10 km. Pluses denote the seismic stations.

wave velocity at a depth of 1.5 km. The low velocity zone in the upper crust (5 km/s at 1.5 km depth) is consistent with the location of calderas, which are marked by circular low Bouguer anomalies (Geological Survey of Japan, 1996).

Magma chambers forming these calderas were located at some depths beneath these areas. The volcanic activity related to felsic calderas ended ca. 1.8 Ma. We can estimate a period of its cooling from the equation of heat conduction. Assuming that the temperature of magma is 800 °C, that the temperature at a depth of 10 km is 450 °C now derived from Curie point temperature and Curie depth (Okubo et al., 1989), and that the temperature gradient and the thermal diffusivity are 25 °C/km and 1.0 mm^2/s, respectively, derived from the typical value in the crust (Turcotte and Schubert, 1982), it took 2 My to cool the rock. Now the magma chamber is cooled enough to solidify the magma.

The low velocity zones are estimated to have relatively high temperature. These may have relation with the calderas. The magma chambers forming the calderas A and B in Fig. 6e seems to be linked together at depths of 10–15 km. The relation between magma chamber of the caldera B and that of the caldera C is not clear. Low velocity zones of the magma chamber of caldera B and that of the caldera D are horizontally separated by high velocity zone.

There should be a penetration of magma from magma chamber to surface calderas. However, these conduits are commonly too narrow to be resolved by the tomographic method.

7.3. Low velocity beneath the Ou Backbone Range

We have obtained a detailed image of the crustal velocity structure beneath the Ou Backbone Range, which is bounded by the Sen'ya and the Uwandaira active faults. We can consider that the reason for the low velocity zone is heat; however, is it sufficient to give the low velocity? Hirata et al. (1999) and Sato et al. (2002) identified the active fault zones using reflection seismic data (Fig. 6c). The 8–10% low velocity zone beneath the Ou Backbone Range coincides with an electrically conductive zone identified in magnetotelluric data (Ogawa et al., 2001). They interpreted this conductor as fluid considering the seismic scatterers identified from natural earthquakes and active sources (Asano et al., 1999). These correlations suggest that the mid-crustal low velocity zone may be related to the presence of fluids.

Pre-Neogene rocks cropping out in the Ou Backbone Range are mainly Cretaceous granitic rocks, and felsic volcanic activity has been dominated in 15–2 Ma (Sato, 1994). Thus the large part of the upper crust is estimated be granitic rocks. A temperature of 680 °C can decrease the velocity by approximately 9% if the cause is only the heat (Fielitz, 1971). However, it is unusual that the zone at a depth of 10 km is over 600 °C where there is no active volcano and the temperature at a depth of 10 km is 450 °C derived from Curie point temperature and Curie depth (Okubo et al., 1989). We cannot explain the low velocity only with heat.

The V_P/V_S ratios of 1.65–1.70 (Fig. 6c) observed here are lower than that of solid granite (1.70; Christensen, 1996). If there is partially molten rock, the V_P/V_S ratios should be larger than 1.90. Therefore we conclude that the low velocities can be attributed to free aqueous fluids rather than molten rock in the middle crust (Mavko, 1980; Takei, 2002; Watanabe, 1994).

Takei (2002) solved the relationship among a ratio of the fractional changes in V_S and V_P, the bulk modulus, and aspect ratio. We can estimate the fraction of liquid using representative values for the P- and S-wave velocities of 6.27 km/s (8.3% lower than solid granite) and 3.68 km/s (5.16% lower), respectively, and a range of V_P/V_S ratios of 1.65–1.70 into expressions recently obtained by Takei (2002). The resulting estimate of the liquid volume fraction is 0.3–5%. The low velocity zone extends about 18 km from north to south with a width of about 10 km in E–W direction and a thickness of about 8 km (Fig. 6a,e).

8. Conclusion

Observations made with a dense seismometer array have elucidated the crustal velocity structure beneath the Ou Backbone Range. The low velocity zone corresponds to shallow Curie depth. Thus the temperature of the low velocity zone can be considered to be high. The low velocity zone beneath the Ou Backbone Range coincides with an

electrically conductive zone detected during a previous magnetotelluric study, and appears to be bounded by the active Sen'ya and Uwandaira faults. We conclude that the low P- and S-wave velocities and small V_P/V_S ratios can be attributed to the presence of free aqueous fluids in the middle crust, and estimate the liquid volume fraction to be 0.3–5%. The low velocity zone extends about 18 km from north to south with a width of about 10 km in E–W direction and a thickness of about 8 km.

Acknowledgments

We are very grateful to Hiroko Hagiwara, who identified the many of 448 earthquakes recorded by the telemetered stations and discuss our results. We wish to acknowledge Takaya Iwasaki, Mitsuhiro Matsu'ura, and Kazuki Koketsu for many valuable comments. We are also grateful to Dapeng Zhao for original tomographic code, to Hiroaki Negishi for helpful advice regarding smoothing, and to Akira Hasegawa, Norihiko Umino and Jun'ichi Nakajima for discussions. The data used in this study were obtained as part of the Joint Seismic Observation under the auspices of the Program for the Study and Observation of Earthquake Prediction, and the Research Group for Explosion Seismology. We used the digital data of traveltimes from 10 shots by the RGES in 1997. We are very grateful to Martha Savage and an anonymous reviewer for useful comment and corrections for our manuscript. The Earthquake Information Center also made available the computing facilities used in this work.

References

Ague, J.J., Park, J., Rye, D.M., 1998. Regional metamorphic dehydration and seismic hazard. Geophys. Res. Lett. 25, 4221–4224.

Asano, Y., Umino, N., Nakamura, A., Okada, T., Hori, S., Kono, T., Nida, K., Sato, T., Hasegawa, A., Kosuga, M., Hasemi, A., 1999. Spatial distribution of seismic scatterers beneath the Ou Backbone Range, Northeastern Japan, estimated by seismic array observation. Zisin, J. Seismol. Soc. Jpn. 52, 79–394 (in Japanese).

Christensen, N.I., 1996. Poisson's ratio and crustal seismology. J. Geophys. Res. 101, 3139–3156.

Fielitz, K., 1971. Elastic wave velocities in different rocks at high pressure and temperature up to 750 degree. Z. Geophys. 37, 943–956.

Geological Survey of Japan, 1996. Gravity map of Kitakami District (Bouguer anomalies). Gravity map series, 6.

Hasegawa, A., 1999. Summary: transect of the northeastern Japan arc–arc deformation and crustal activity. Earth Mon. Spec. 27, 5–11 (in Japanese).

Hirata, N., Sato, H., Iwasaki, H., Krashimo, E., 1999. Deep seismic reflection profiling across the Ou backbone range. Earth Mon. Spec. 27, 39–43 (in Japanese).

Hori, S., Umino, N., Hasegawa, A., 1999. Distribution of S-wave reflector in the southern part of Tohoku district, northeastern Japan. Earth Mon. Spec. 27, 155–160 (in Japanese).

Iwasaki, T., Kurashimo, E., Hirata, N., Moriiya, T., Demachi, T., Okada, T., Miyamachi, H., 1999. Crustal structure and beneath the eastern part of Backbone Range, northern Honshu, Japan by seismic refraction experiment. Prog. Abst. Seismol. Soc. Jpn. 2, B45 (in Japanese).

Iwasaki, T., Kato, W., Moriya, T., Hasemi, A., Umino, N., Okada, T., Miyashita, K., Mizogami, T., Takeda, T., Sekine, S., Matsushima, T., Tashiro, K., Miyamachi, H., 2001. Extensional structure in northern Honshu Arc as inferred from seismic refraction/wide-angle reflection profiling. Geophys. Res. Lett. 28, 2329–2332.

Matsubara, M., Hirata, N., Sakai, S., Hagiwara, H., 2001. Three-dimensional P- and S-wave velocity structure in the backbone range of Tohoku, northeast Japan, by a traveltime inversion method with spatial correlation of velocities. Prog. Abst. Seismol. Soc. Jpn. 2, C27 (in Japanese).

Mavko, G., 1980. Velocity attenuation in partially molten rocks. J. Geophys. Res. 85, 5173–5189.

Nakajima, J., Matsuzawa, T., Hasegawa, A., Zhao, D., 2001. Three-dimensional structure of V_P, V_S and V_P/V_S beneath northeastern Japan: implications for arc magmatism and fluids. J. Geophys. Res. 106, 21843–21857.

Ogawa, Y., Mishina, M., Goto, T., Satoh, H., Oshiman, N., Kasaya, T., Takahashi, Y., Nishitani, T., Sakanaka, S., Uyeshima, M., Takahashi, Y., Honkura, Y., Matsushima, M., 2001. Magneto-telluric imaging of fluid in intraplate earthquake zones, NE Japan back arc. Geophys. Res. Lett. 28, 3741–3744.

Okubo, Y., Tsu, H., Ogawa, K., 1989. Estimation of Curie point temperature and geothermal structure of island arcs of Japan. Tectonophysics 159, 279–290.

Research Group for Explosion Seismology (RGES), 1999. Seismic refraction/wide-angle experiment across the northern Honshu arc. Bull. Earthq. Res. Inst. Univ. Tokyo 74, 63–122 (in Japanese).

Research Group for the Seismicity and Structure of NE Honshu, Japan, 1998. Joint Seismic Observation and Prospecting in Tohoku, NE Japan, Prog. Abstr. Japan Earth and Planet. Sci. 1998 Joint meeting, p. S–84 (in Japanese).

Sato, H., 1994. The relationship between late Cenozoic tectonic events and stress field and basin development in northeast Japan. J. Geophys. Res. 99, 22261–22274.

Sato, H., Amano, K., 1991. Relationship between tectonics, volcanism, sedimentation and basin development, Lake Cen-

ozoic, central part of Northern Honshu, Japan. Sediment. Geol. 74, 323–343.

Sato, H., Hirata, N., Iwasaki, T., Matsubara, M., Ikawa, T., 2002. Deep seismic reflection profiling across the Ou Backbone range, northern Honshu Island, Japan. Tectonophysics 355, 41–52.

Takei, Y., 2002. Effect of pore geometry on V_P/V_S: from equilibrium geometry to crack. J. Geophys. Res. 107 (B2), 2043, doi:10.1029/2001JB000522.

Turcotte, D.L., Schubert, G., 1982. Geodynamics, applications of continuum physics to geological problems. Wiley, Canada.

Urabe, T., 1994. A common format for multi-channel earthquake waveform data. Prog. Abst. Seismol. Soc. Jpn. 2, 384 (in Japanese).

Watanabe, T., 1994. Melt beneath volcanoes—inference from seismic velocities. Mem. Geol. Soc. Jpn. 43, 20–31 (in Japanese with English abstract).

Yamasaki, N., 1896. Preliminary report of the Riku-u earthquake. Rep. Imp. Earthq. Invest. Comm. 11, 50–74 (in Japanese).

Yoshida, T., 2001. The evolution of arc magmatism in the NE Honshu arc, Japan. Tohoku Geophys. J. 36, 131–149.

Zhao, D., Hasegawa, A., 1993. P wave tomographic imaging of the crust and upper mantle beneath the Japan islands. J. Geophys. Res. 98, 4533–4534.

Zhao, D., Hasegawa, A., Horiuchi, S., 1992. Tomographic imaging of P and S wave velocity structure beneath Northeastern Japan. J. Geophys. Res. 97, 19909–19928.